# Determination of elastic constants and rotational viscosity of micellar liquid crystals by conductivity measurements

J. Bajc, G. Hillig, and A. Saupe

Citation: The Journal of Chemical Physics **106**, 7372 (1997); doi: 10.1063/1.473698
View online: http://dx.doi.org/10.1063/1.473698
View Table of Contents: http://scitation.aip.org/content/aip/journal/jcp/106/17?ver=pdfcov
Published by the AIP Publishing

# Determination of elastic constants and rotational viscosity of micellar liquid crystals by conductivity measurements

J. Bajc,[a] G. Hillig, and A. Saupe
*Max-Planck-Society Research Group Liquid Crystal Systems at Martin-Luther University, Mühlpforte 1, 06 108 Halle, Germany*

(Received 3 January 1997; accepted 30 January 1997)

An experimental study of a lyotropic nematic liquid crystal (CsPFO in a water solution) confined to a cylindrical tube is presented. The structure of the sample is controlled by a magnetic field. A small ac voltage is applied along the tube for conductivity measurements. Elastic constants and conductivity constants of the material are determined from static measurements at different magnetic fields. The method is also used to determine the rotational viscosity $\gamma_1$ from dynamic response under sudden changes of the magnetic field. The dynamic measurements are analyzed in the framework of the Leslie–Ericksen theory. It is shown that although the dynamic behavior can be qualitatively explained with a single effective rotational viscosity $\gamma_1$, back flow effects have to be taken into account should the analysis yield consistent values for $\gamma_1$. The results obtained by this method agree well with other experimental studies. © *1997 American Institute of Physics.* [S0021-9606(97)52017-4]

## I. INTRODUCTION

The conduction anisotropy of the lyotropic nematic state depends on the size and shape of the micelles, the orientational order, and the temperature.[1] The conductivity measurements, which are presented here, were performed in a cylindrical capillary. For director–surface interaction we assume a strong homeotropic anchoring. In equilibrium the radial escape mode builds up, where director ''escapes'' along the cylinder axis [Fig. 1(a)]. The susceptibility anisotropy of the nematic CsPFO solution is positive and the nematic director tends to align parallel to the magnetic field. If the field is applied along the cylinder axis the escaped structure is deformed [Fig. 1(b)], whereas if a strong enough field is applied perpendicular to the tube a different structure with a director lying in a plane perpendicular to the tube axis may be the most stable one [Fig. 1(c)]. The effective conductivity for the magnetic field parallel to the axis reflects the modifications of the escaped structure. These conductivity data are used to determine the splay and bend elastic constant.

Besides the above static experiments, the time dependence of the current after a sudden change of the magnetic field was measured, in order to determine the rotational viscosity $\gamma_1$.

The paper focuses on experimental determination of the conductivity constants, the elastic constants, and the rotational viscosity, and the temperature dependence of these constants in the vicinity of the nematic–lamellar transition. In Sec. II the experimental setup is described. The theoretical background of the observed phenomena is given in Sec. III for the static case and in Sec. IV for the dynamic case. Finally, the results are presented and discussed in Sec. V.

[a]Permanent address: Department of Physics, University of Ljubljana, Jadranska 19, 1000 Ljubljana, Slovenia.

## II. EXPERIMENT

The system under investigation is an anionic surfactant, caesium perfluorooctanoate (CsPFO). At a ratio CsPFO/$H_2O$=49/51 wt.% the system shows a lamellar smectic phase up to 35.5 °C, followed by a nematic phase consisting of disklike aggregates, which transforms at 40.1 °C to an isotropic solution.[2] The nematic–lamellar transition is second order, whereas the nematic–isotropic transition is first order.

The measurements were performed in H-shaped glass cells ($l \approx 50$ mm, $R = 0.30$ mm, 1.25 mm). The cell was used without any special treatment of the inner walls. The discotic micelles tend to lie with their flat side parallel to the tube wall, resulting in a homeotropic anchoring. An ac voltage of a frequency of 1 kHz was applied between the two platinum electrodes at the ends of the tube. The applied voltage was smaller than 0.5 V and the influence of the corresponding electric field on the director orientation could be neglected. The cell constant was determined by filling the cell with the 0.1 N KCl solution. The cell was mounted in a heating stage with a temperature control better than $\pm 1$ mK and positioned in a magnetic field (Bruker, BE10 with $B \leqslant 0.78$ T). We used two orientations of the cell; the tube axis was either parallel or perpendicular to the applied magnetic field.

The nematic and lamellar phase are uniaxial and have two principal conductivities $k_1$ and $k_2$. In Fig. 2 an example of measurements of these in strong magnetic fields is presented. In this case of magnetic coherence length $\xi_m = \sqrt{\mu_0 K_{11}/(\chi_a B^2)}$ is much smaller than the radius of the tube $(R)$. The two principal conductivities, with the field parallel to the tube axis $(k_1)$ and perpendicular to it $(k_2)$ are shown. The measured $k_1$ will differ slightly from the accurate value because a thin film along the surface of the thickness of the magnetic coherence length will remain vertical to the field [Fig. 1(b)].

Homeotropic boundary conditions and positive magnetic

 0021-9606/97/106(17)/7372/6/$10.00 

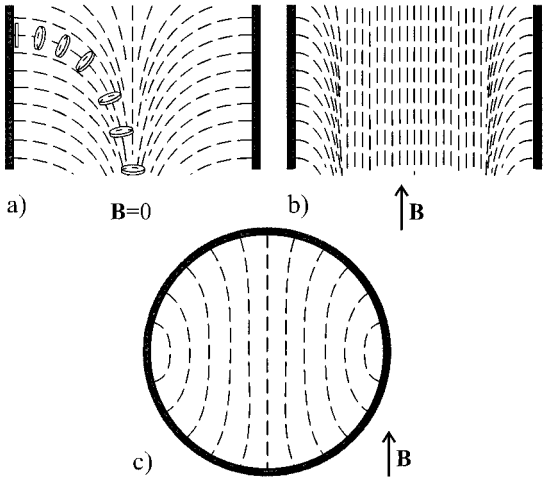


FIG. 1. Schematic presentation of a typical director field in a cylindrical tube, shown in the cross section containing the tube axis (a), (b) and in the cross section perpendicular to the tube axis (c). Sketch (a) shows the so-called radial escape structure, which is stable if no field is applied. A few micelles are added to make sketch more illustrative. Sketch (b) shows modifications of this structure, when a magnetic field is applied along the tube axis. The thickness of the layer, which remains unaligned with the field, is approximately equal to the magnetic coherence length $\xi_m$. If the field is applied perpendicular to the tube, director field shown in sketch (c) may become the most stable. The tickness of the unaligned stripe at the wall is again approximately $\xi_m$.

susceptibility provide the possibility of direct and accurate measurement of $k_2$. Because, when a strong magnetic field is applied perpendicular to the tube axis, a planar structure becomes the most stable structure [Fig. 1(c)]. In the planar configuration the director field $\mathbf{n}(\mathbf{r})$ is perpendicular to the direction of the electric current. As mentioned above a direct and accurate measurement of $k_1$ is not possible. We determined it by extrapolation or by computer fits to field dependent conduction measurements. A combination of measurements at low magnetic fields ($\xi_m \sim R$) and at high fields ($\xi_m \ll R$) was used to determine elastic constants.

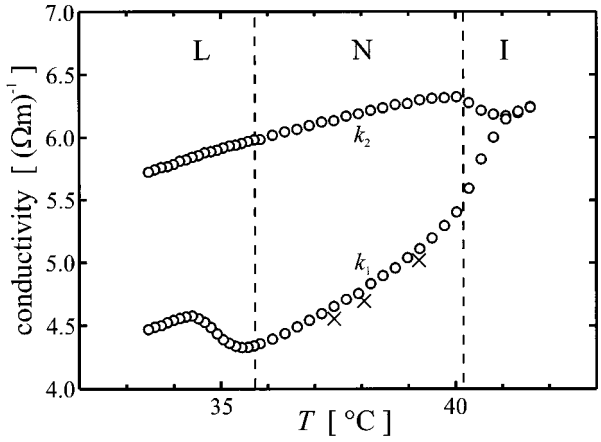


FIG. 2. Principal conductivities $k_1$ (field $\parallel$ axis) and $k_2$ (field $\perp$ axis) for CsPFO/$H_2O$=49/51 wt. % in a cooling sequence (circles). In the isotropic phase the conductivity is independent of the orientation ($k_1=k_2$). Accurate values for $k_1$ (crosses) are few percents below the directly measured ones. In the vicinity of the nematic–isotropic transition the two phases coexist. The right dashed line indicates the temperature below which there is no isotropic phase. The clearing point is approximately 0.8 °C above this temperature.

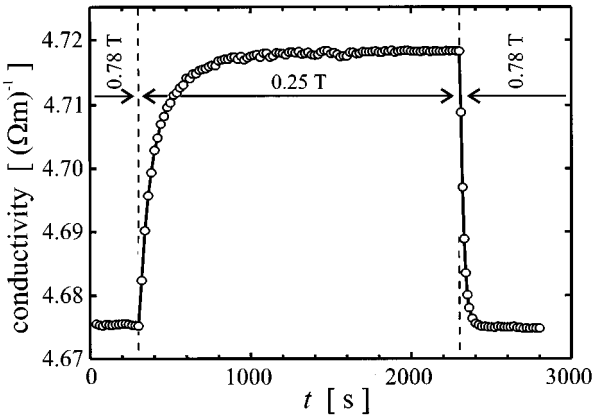


FIG. 3. Measured conductivity $k_1$ vs time after an abrupt change of the magnetic field along the tube. Arrows indicate time intervals with constant magnetic field. Relaxation is faster when the field is increased, because the magnetic torques that act on the entire sample govern the relaxation. On the other hand, when the field is decreased, reorientation of the director is governed by the elastic torques, which are transferred from the unaligned surface stripe towards the inner part of the tube. Therefore the relaxation is slower.

To determine the rotational viscosity $\gamma_1$ we also studied the time dependence of the effective conductivity, following an abrupt change of the strength of the magnetic field. Figure 3 shows an example of the dynamic measurement.

To sum up, we measured the resistance of the cell in dependence of applied magnetic fields for various temperatures. The resistance of the cell was determined by measuring the voltage drop across the cell and the current. The experiment was computer controlled with an automatic data collection.

## III. DETERMINATION OF ELASTIC CONSTANTS

In the static case the director field $\mathbf{n}(\mathbf{r})$ is determined by the Frank–Oseen free energy density[3,4]

$$f=\frac{1}{2}\left\{K_{11}(\nabla\cdot\mathbf{n})^2+K_{22}[\mathbf{n}\cdot(\nabla\times\mathbf{n})]^2+K_{33}|\mathbf{n}\times(\nabla\times\mathbf{n})|^2 - \frac{\chi_a}{\mu_0}(\mathbf{B}\cdot\mathbf{n})^2\right\}, \quad (1)$$

where $K_{11}$, $K_{22}$, and $K_{33}$ are splay, twist, and bend elastic constants, respectively, and $\chi_a$ is the magnetic anisotropy. In our case $\chi_a>0$ and preferred orientation of the director is parallel to the applied magnetic field $\mathbf{B}$.

A general remark about different influences (such as electric or magnetic fields, presence of bounding surfaces, etc.) that modify the liquid crystal structure is appropriate at this point. In order to compare these interactions characteristic lengths are introduced; the magnetic coherence length $\xi_m$ and the electric coherence length $\xi_e=\sqrt{K_{11}/(\epsilon_a\epsilon_0 E^2)}$.

They scale the distance from the surface over which the director field is realigned by an external field. Smaller lengths correspond to stronger interactions. In the studied case, electric fields were weak ($\xi_e \gg R$) and we can neglect their influence on the structure. On the other hand, the magnetic field varied from low values ($\xi_m \gtrsim R$) to very high values ($\xi_m \ll R$).

As explained above, the measured conductivity is dependent on the applied field when the orientation of the magnetic field is parallel to the tube axis. The field does not break the symmetry, so we can use cylindrical coordinates and the ansatz for the director field reads

$$\mathbf{n}=\sin(\Omega)\hat{e}_\varrho+\cos(\Omega)\hat{e}_z, \tag{2}$$

where the angle $\Omega$ is a function of radial coordinate $x\equiv\varrho/R$. The ansatz (2) results in zero twist contribution to the free energy, therefore the structure is not dependent on the twist elastic constant $K_{22}$. In the equilibrium the sum of elastic and magnetic torques, acting on **n**, is equal to zero, resulting in the differential equation

$$\Gamma_e+\Gamma_m=\frac{K_{11}}{R^2}\left\{(\cos^2\Omega+\beta_3\sin^2\Omega)\frac{(x\Omega')'}{x} - \sin\Omega\cos\Omega\left[\frac{1}{x^2}+\left(\frac{R}{\xi_m}\right)^2 + (1-\beta_3)(\Omega')^2\right]\right\}=0, \tag{3}$$

where $\beta_3\equiv K_{33}/K_{11}$ is the ratio of the bend and splay elastic constant. The derivative with respect to $x$ is denoted by a prime $\Omega'\equiv\partial\Omega/\partial x$. The differential equation (3) is solved numerically using the relaxation method.[5] The method is based on successive changes of the starting configuration. The correction of the function $\Omega$ at a certain point $x$ is proportional to the torque at this point, i.e., the method imitates the physical process of relaxation. The important difference is that in real relaxation processes the time rate is fixed, whereas in the relaxation method the steps are adjusted so that the equilibrium, i.e., the solution of the differential equation, is reached by making as few steps as possible. This method is suitable, because the structures at several successive magnetic fields are to be calculated and solution at a certain field is taken as the first approximation for the structure at the following field. The method converges fast for the changes of the field up to 0.1 T.

The total electric current $I$ through the capillary reads

$$I=\int \mathbf{j}\cdot d\mathbf{S} =I_0\int_0^1\left[1+\frac{(k_2-k_1)\sin^2\Omega(x)}{k_1\sin^2\Omega(x)+k_2\cos^2\Omega(x)}\right]2x\,dx, \tag{4}$$

where $I_0=\pi R^2 k_1 E$. The calculated dependence of electric current on the applied magnetic field (Fig. 4) shows that at sufficiently low fields a ''plateau'' is reached, because the elastic torques dominate. Behavior in this range is sensitive to ratio, $\beta_3=K_{33}/K_{11}$. For high fields the influence of $k_2$, the conductivity perpendicular to the director, is fading away (as $1/B$) and the resulting current approaches $I_0$. Precise measurements in this range give accurate values for $k_1$, but are not very sensitive to the ratio $\beta_3$. Combination of measurements at low and high magnetic fields provides enough information for accurate determination of all three parameters, $K_{11}$, $K_{33}$, and $k_1$ (see Fig. 4). The fourth material constant in question, $k_2$, has to be determined by a separate measurement with the field perpendicular to the tube axis.

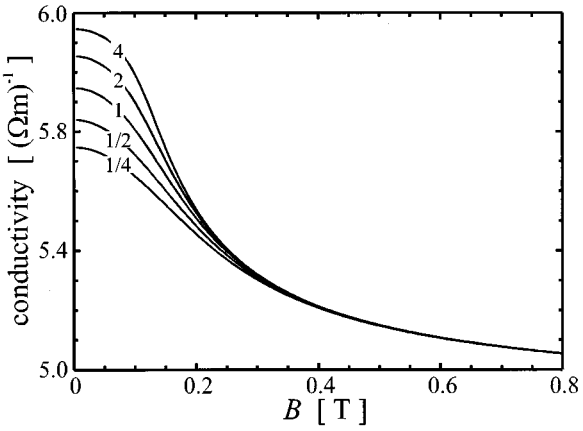


FIG. 4. Dependence of the conductivity on magnetic field $B$ for several ratios $K_{33}/K_{11}$. The magnitude of the elastic constants only scales the $B$ axis [see $\xi_m$ and Eq. (3)] and is adjusted in such a way to demonstrate the weak dependence of the curves on $K_{33}/K_{11}$ at high fields. In reality the constants are determined from the experiments, and upper graph clearly shows that measurements at high fields are not sufficient.

## IV. DETERMINATION OF ROTATIONAL VISCOSITY

Let us first neglect the back flow and take a look at simplified description of a director's reorientation process with a single effective rotational viscosity $\tilde{\gamma}_1$.

In an equilibrium director field, the net torque on the director equals zero at each point. In other words, the elastic torques are balanced by, for example, the magnetic ones. When the director field is out of equilibrium, a net torque rotates the director into the equilibrium position. Neglecting the back flow effects,[6] the torque balance gives

$$\tilde{\gamma}_1\dot{\Omega}=\Gamma_e+\Gamma_m, \tag{5}$$

where $\dot{\Omega}$ is the angular velocity of the director (the dot indicates the derivative with respect to time $\dot{\Omega}\equiv\partial\Omega/\partial t$). The sum of elastic and field torques is given in Eq. (3).

If we start with an equilibrium structure ($\dot{\Omega}=0$) and change the magnetic field abruptly, the coherence length $\xi_m$ changes and $\Gamma_e+\Gamma_m$ is no longer zero. The director rotates towards the new equilibrium orientation with the angular velocity $\dot{\Omega}$, proportional to the torque. The time dependence of $\Omega$ is obtained by numerical integration of Eq. (5).

A complete set of equations that takes the coupling between the director reorientation and the mass flow into account involves five independent viscosity coefficients.[7,8] Again we assume that the solution has cylindrical symmetry and that it is independent of $z$ and the azimuthal angle $\phi$. It implies

$$\mathbf{v}=v(x)\hat{e}_z. \tag{6}$$

In this case the Leslie–Ericksen equations for an incompressible nematic-liquid crystal reduce to

$$\dot{w}=\frac{1}{x\tau_0}\{x[K(\Omega)w'+M(\Omega)\dot{\Omega}]\}', \tag{7}$$

$$\dot{\Omega}=\frac{1}{\tau}\left\{(\cos^2\Omega+\beta_3\sin^2\Omega)\frac{(x\Omega')'}{x} -\sin\Omega\cos\Omega\left[\frac{1}{x^2}+\left(\frac{R}{\xi_m}\right)^2+(1-\beta_3)(\Omega')^2\right]\right\} -M(\Omega)w', \tag{8}$$

where $w\equiv v/R$ is the velocity reduced to the tube radius, $\tau_0\equiv\rho R^2/\gamma_1$ is the characteristic time for the velocity relaxation, $\rho$ is the density of the liquid crystal, and $\tau\equiv\gamma_1 R^2/K_{11}$ is the characteristic time for the director reorientation. Eq. (7) is the equation of motion, whereas Eq. (8) results from the balance of torques. The coefficients $K$ and $M$ read

$$M(\Omega)=\frac{1}{2}\left[1+\frac{\eta_2-\eta_1}{\gamma_1}\cos(2\Omega)\right], \tag{9}$$

$$K(\Omega)=\frac{\alpha_1}{\gamma_1}\sin^2\Omega\cos^2\Omega+\frac{\eta_1}{\gamma_1}\sin^2\Omega+\frac{\eta_2}{\gamma_1}\cos^2\Omega, \tag{10}$$

where $\alpha_1$, $\eta_1$, $\eta_2$, and $\gamma_1$ are the four independent viscosity coefficients. The shear viscosity, $\eta_3$, does not enter the equations.

The time scales in Eqs. (7) and (8) are several orders of magnitude away from each other, i.e., $\tau_0/\tau=\rho K_{11}/\gamma_1^2\ll 1$. It follows, that the velocity field relaxes very quickly for any director rotation. In other words, the left-hand side of Eq. (7) can be set to zero. The expression in braces is therefore a function of time only

$$K(\Omega)w'+M(\Omega)\dot{\Omega}=\frac{F(t)}{x}. \tag{11}$$

If $F(t)$ is not zero, $w'$ becomes infinite in the center of the capillary. It follows that $F(t)\equiv 0$ and $w'=-M(\Omega)\dot{\Omega}/K(\Omega)$. Equation (8) thus reads

$$\left[1-\frac{M^2(\Omega)}{K(\Omega)}\right]\dot{\Omega}=\frac{1}{\tau}\left\{(\cos^2\Omega+\beta_3\sin^2\Omega)\frac{(x\Omega')'}{x} -\sin\Omega\cos\Omega\left[\frac{1}{x^2}+\left(\frac{R}{\xi_m}\right)^2+(1-\beta_3)(\Omega')^2\right]\right\} \tag{12}$$

and can be integrated numerically with the same ease as Eq. (5). The expression $\gamma_1[1-M^2(\Omega)/K(\Omega)]$ can be identified as the effective viscosity $\tilde{\gamma}_1$ and should therefore be positive. This constrains the range of allowed values of the viscosity coefficients.

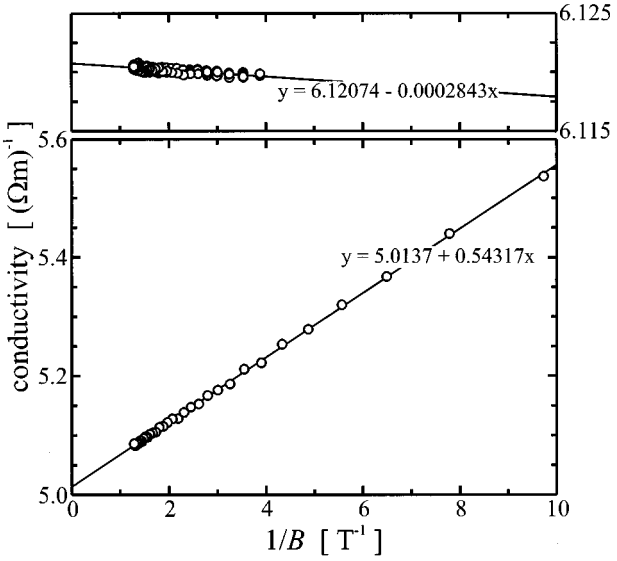


FIG. 5. Measured conductivities as a function of $1/B$. (The lower part) **B** parallel to the tube axis, $T=39.219$ °C. Well defined slope at high fields confirms the $1/B$ dependence of the unaligned film at the wall. Extrapolation of fitted linear function to $1/B=0$ gives the corrected value of $k_1$. (The upper part) **B** perpendicular to the tube axis, $T=38.036$ °C. No significant dependence is noticeable. The slope of the fitted linear function is four orders of magnitude smaller than the slope in the first case, and even this can be, to some extend, ascribed to the temperature changes, induced by the field changes. Note that $y$ scale on the upper plot is 20 times smaller than the scale on the lower one.

## V. MEASUREMENT ANALYSIS AND RESULTS

The conductivity perpendicular to the director, $k_2$ has been measured directly with an accuracy $\sim 10^{-4}$ (Figs. 2 and 5). The conductivity parallel to the director, $k_1$ was obtained in two ways. The simplest way is by an extrapolation of the measured conductivity (see Fig. 5). The $k_2$ contribution to the measured conductivity is proportional to the volume of the unaligned film at the tube wall. Therefore its asymptotic behavior in a strong magnetic field is proportional to $1/B$ and extrapolation to $B\to\infty$ results in an accurate value for $k_1$.

The other possible way to obtain $k_1$ is by fitting the measured conductivity dependence in the entire range of applied magnetic fields, which is primarily done to obtain the elastic constants $K_{11}$ and $K_{33}$. It turned out, that calculated conductivity dependencies fitted the measurements much better, if besides $K_{11}$ and $K_{33}$ the $k_1$ was varied as a fitting parameters as well, i.e., the method showed significant sensitivity for $k_1$. Therefore all three parameters were adjusted. The resulting $k_1$ values are close to those, obtained by the extrapolation, but they are determined with better accuracy. Figure 6 shows a typical example of a fitted curve for the smaller capillary ($R=0.3$ mm) at the temperature $T=39.219$ °C. The estimated error of the $k_2$ values is below 0.2%, whereas the error of the obtained $k_1$ values is a bit larger, up to 0.5%. A general difficulty of the lyotropic system is the loss of water that results in changes of the characteristic properties with time. Over a few months, we noticed a drift of $k_2$ and $k_1$, approximately 0.5% and 3%,

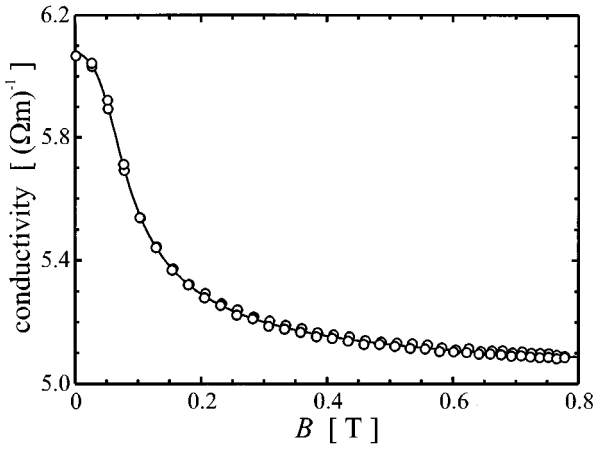


FIG. 6. Comparison of the fitted curve (solid line) and the experimental data (circles) for the temperature 39.219 °C and the capillary radius $R = 0.3$ mm. The curves superimpose well in the entire range.

respectively. The transition temperature drifted for approximately 0.4 °C.

As described above, the measurements at low magnetic fields are required for accurate determination of both elastic constants. The problem with these measurements is slow relaxation, i.e., the time between successive measurements may go beyond reason. On the one hand, $R$ should be small, to enable quick measurements at low fields, on the other hand, the maximal strength of the magnet limits us to radii that are large with respect to the minimal coherence length $\xi_m^0 = \sqrt{\mu_0 K_{11}/(\chi_a B_0^2)}$. In our case $B_0 = 0.78$ T and $\xi_m^0 \approx 10\ \mu$m at 39 °C and it becomes larger with decreasing temperature.

With a tube with $R = 1.25$ mm measurements below 0.15 T were not possible. With a smaller tube ($R = 0.3$ mm) we were able to measure down to zero magnetic field and we obtained accurate values for both elastic values. With the larger tube we nevertheless checked the consistency of the measurements; we fixed one of the elastic constants to the value obtained by the optical Frederiks experiments[9] and adjusted the other one and $k_1$. The values for the elastic constants are in reasonable agreement with the ones obtained with the smaller tube (see Fig. 7), and the matching of the $k_1$ values is excellent.

The temperature dependence of the elastic constants is given in Fig. 7. A strong increase of $K_{33}$ in the investigated range indicates that the bend elastic constant diverges in the vicinity of the nematic–lamellar phase transition. On the other hand, $K_{11}$ shows a noncritical behavior and is less temperature dependent. Both elastic constants are in good agreement with the values obtained by optical measurements, if the same susceptibility anisotropy is used. Namely, what we get from the measurements are the ratios $K_{11}/\chi_a$ and $K_{33}/\chi_a$ [see expression for $\xi_m$ and Eq. (3)]. In order to obtain the elastic constants we used the $\chi_a$ values from the optical experiments. The possible resulting systematic error is limited to few percents, because the temperature dependence of $\chi_a$ is weak.[9] The estimated overall error of the obtained elastic constants is below 10%.

The dynamic response of the conductivity (Fig. 3) was analyzed in two steps. First we fitted the measurements without inclusion of the back flow effects and thereby gained two effective rotational viscosities $\tilde{\gamma}_1$, one for decreasing and one for increasing the field. If the back flow could be neglected, the two values would be the same—equal to real rotational viscosity $\gamma_1$. But we obtained two very different

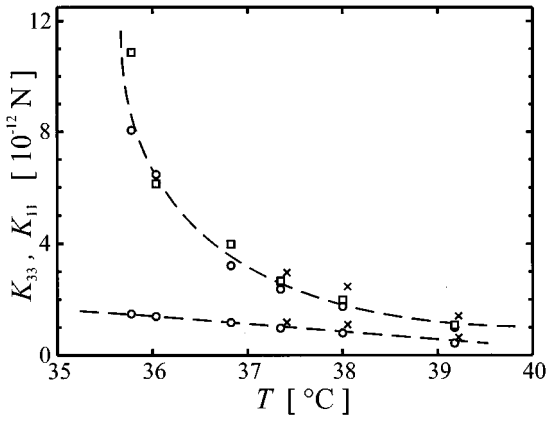


FIG. 7. Temperature dependence of splay and bend elastic constants. The upper points show $K_{33}$ and the lower ones $K_{11}$. The data from optical measurements are denoted with circles (Ref. 9). The values obtained with the smaller capillary ($R = 0.3$ mm) are denoted with crosses, the ones obtained with the larger one ($R = 1.25$ mm) are denoted with squares. In this case the $K_{33}$ values were derived with $K_{11}$ values, taken from optical measurements, because we could not measure at low magnetic fields. Characteristic behavior of both constants is indicated by the dashed lines; $K_{33}$ diverges near the lamellar–nematic transition, whereas $K_{11}$ does not show any critical behavior.

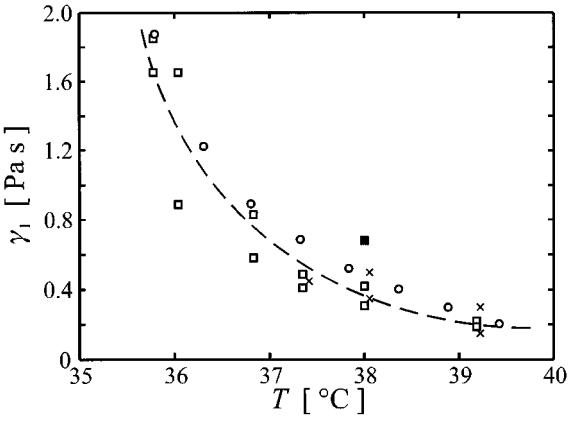


FIG. 8. Temperature dependence of the rotational viscosity. The values of the effective rotational viscosity obtained with the smaller capillary ($R = 0.3$ mm) are denoted with crosses, the ones obtained with the larger one ($R = 1.25$ mm) are denoted with squares. At each temperature there are two effective viscosities, $\tilde{\gamma}_{1\uparrow}$ and $\tilde{\gamma}_{1\downarrow}$, the later being always smaller than the former. The filled square denotes the $\gamma_1$ value at $T = 38.001$ °C, obtained from $\tilde{\gamma}_1$ values at this temperature when back flow is taken into account. The divergent behavior in the vicinity of the lamellar–nematic transition is indicated by the dashed line. For comparison, the rotational viscosities obtained by optical measurements (Ref. 9) are added (circles).

values, for example $\tilde{\gamma}_{1\uparrow}=0.42$ Ns/m$^2$ for the increase of the field and $\tilde{\gamma}_{1\downarrow}=0.31$ Ns/m$^2$ for the decrease of the field, both at $T=39.219$ °C. This is a clear indication that $\gamma_1$ can be determined accurately only if the analysis includes the back flow effects.

In the next step we tried to determine how much does the back flow change the results. There are four parameters to adjust ($\alpha_1$, $\eta_1$, $\eta_2$, and $\gamma_1$). In order to obtain an estimate of the influence of the back flow, we set $\alpha_1\equiv 0$ and assumed several values for $\eta_1$, $\eta_2$, and $\gamma_1$. Comparison of simulated relaxation with and without back flow resulted in corrected values for the rotational viscosity. For example, with $\eta_1/\gamma_1=1/3$ and $\eta_2/\gamma_1=4/3$ we got $\gamma_{1\uparrow}=0.678$ Ns/m$^2$ for the increase of the field and $\gamma_{1\downarrow}=0.686$ Ns/m$^2$ for the decrease of the field, both at $T=39.219$ °C. The agreement between $\gamma_{1\uparrow}$ and $\gamma_{1\downarrow}$ is indeed much better.

The temperature dependence of $\tilde{\gamma}_1$ is shown in Fig. 8. The data agree qualitatively with $\gamma_1$ values which were obtained by optical measurements at planar surfaces.[9]

## ACKNOWLEDGMENTS

Financial support from the German–Slovene bilateral collaboration ''Fluessigkristalle'' (Grant No. 6.BOA.1.A), Slovenian Ministry of Science and Technology (Grant No. J1-7067), and Max-Buchner research Grant No. 1885 are gratefully acknowledged.

[1] P. J. Photinos and A. Saupe, J. Chem. Phys. **84**, 517 (1986).
[2] N. Boden and M. C. Holmes, Chem. Phys. Lett. **109**, 76 (1984).
[3] F. C. Frank, Discuss Faraday Soc. **25**, 19 (1958).
[4] C. W. Oseen, Trans. Faraday Soc. **29**, 883 (1933).
[5] W. H. Press, B. P. Flannery, S. A. Teukolsky, and W. T. Vetterling, *Numerical Recipes* (Cambridge University Press, Cambridge, 1992).
[6] P. G. de Gennes and J. Prost, *The Physics of Liquid Crystals* (Oxford University Press, Oxford, 1993).
[7] J. L. Ericksen, Archs. Ration. Mech. Anal. **4**, 231 (1960); Phys. Fluids **9**, 1205 (1966).
[8] F. M. Leslie, Q. J. Mech. Appl. Math. **19**, 357 (1966); Archs. Ration. Mech. Anal. **28**, 265 (1968).
[9] S.-S. Pak, dissertation, Kent State University, 1994.